2018

TRANSIENT SIMULATIONS OF FRESHWATER LENS DEPLETION IN RESPONSE TO A RANGE OF SEA LEVEL RISE RATES AND CLIMATE GRADIENTS

Qiuyuan Nan
qnan@mtu.edu

TRANSIENT SIMULATIONS OF FRESHWATER LENS DEPLETION IN RESPONSE TO A RANGE OF SEA LEVEL RISE RATES AND CLIMATE GRADIENTS

By

Qiuyuan Nan

A REPORT

Submitted in partial fulfillment of the requirements for the degree of

MASTER OF SCIENCE

In Environmental Engineering

MICHIGAN TECHNOLOGICAL UNIVERSITY

2018

This report has been approved in partial fulfillment of the requirements for the Degree of MASTER OF SCIENCE in Environmental Engineering.

Department of Civil and Environmental Engineering

Report Advisor:	*Alex S. Mayer*
Committee Member:	*John S. Gierke*
Committee Member:	*Jason Gulley*
Department Chair:	*Audra N. Morse*

Table of Contents

List of figures

List of tables

Acknowledgements

I want to give my sincere thanks to Dr. Alex Mayer, who had guided me through the pursuit of the M.S. degree and helped me whenever I got lost. I have the most profound respect and appreciation for him.

During the preparation of the report, I got detailed advice from my committee members. I would like to extend my sincere thanks to Dr. John Gierke and Dr. Jason Gulley for giving me their kind assistance and serving as committee members.

During this study, I also got the help from many faculties from different department and institution. Here I want to thank Mr. Vivek Bedekar from S.S. Papadopulos & Associates, Inc., who helped me establish the numerical model in SEAWAT, and Dr. Shiliang Wu from Michigan Tech, who gave me lots of advice in my study and life.

Special thanks to my parents for their caring and support for my Master's Degree study.

Abstract

The freshwater lens in the island can become the only freshwater resources in some regions. Numerical simulations are used to determine freshwater lens volume and average concentration is in response to the range of sea-level rise rates and climate gradients. The sea-level rise rates (0.56 mm/yr, 6.22 mm/yr, and 11.78 mm/yr) are selected for projected and the climate gradient is computed from the islands in the Bahamian archipelago (Inagua, San Salvador, and Grand Bahamas) in the north, central and south. Based on the simulation results, all cases presented the upward trend of the average salinity but have the oscillation in their 1-year cyclical period. The magnitude of the oscillation changed to accord with the season climate condition. The cases with 11.78mm sea-level rise rate usually have the highest slope in salinity vs. time plot, which means the fastest freshwater lens depletion. The cases with 0.56mm sea-level rise rate have the slowest upward trend which the slope almost equal to 0. The lake expansion scenarios also have a larger slope than the non-lake expansion scenarios. The initial position of the average concentration in Inagua Island is higher than the other two islands because Inagua Island has the driest climate condition so that the initial freshwater lens volume is smaller than the other two islands. Only Grand Bahama Island has a positive recharge in the lake, land and entire island for all three sea-level rise situations and Inagua Island has the largest negative recharge value of the lake. Higher sea-level rise rate would lead to faster lake expansion and land loss.

1 Main body

1.1 Introduction

Freshwater resources are one of the essential resources for the survival of humans and other living things. Although water covers most of the Earth's area, only 3% of it is freshwater. As an essential part of freshwater resources, groundwater accounts for 30% of freshwater resources. Groundwater is not only stored in inland areas but also stored in island and coastal aquifers. Therefore, seawater intrusion for coastal aquifer is a common phenomenon all over the world that cause serious influence on groundwater (Barlow and Reichard, 2010; Santha Sophiya and Syed, 2013; Green and Macquarrie, 2014; Xu et al., 2016; Abd-Elhamid, 2017; Huang and Yung-Chia Chiu, 2018; Kalaoun, Jazar & Bitar, 2018).

The freshwater lens is a wedge-shaped body overlying the saltwater portion of island aquifers and has a mixing zone for freshwater and seawater exchange as the boundary (Fratesi, 2013, see Figure 1-1). Since the freshwater lens is the only freshwater resource on small islands, it is critical to understand the factors affecting the freshwater lens dynamics. On an island, the only source of freshwater is the rainfall at the land surface, so that has the name called autogenic recharge. On the other hand, due to the dynamic exchange in the mixing zone, the concentration and volume of the freshwater lens are affected by the seawater. The shape of the freshwater lens is modified by the recharge and hydraulic conductivity and be segmented by evaporative lakes (Vacher and Mylroie, 1991; Fratesi, 2013).

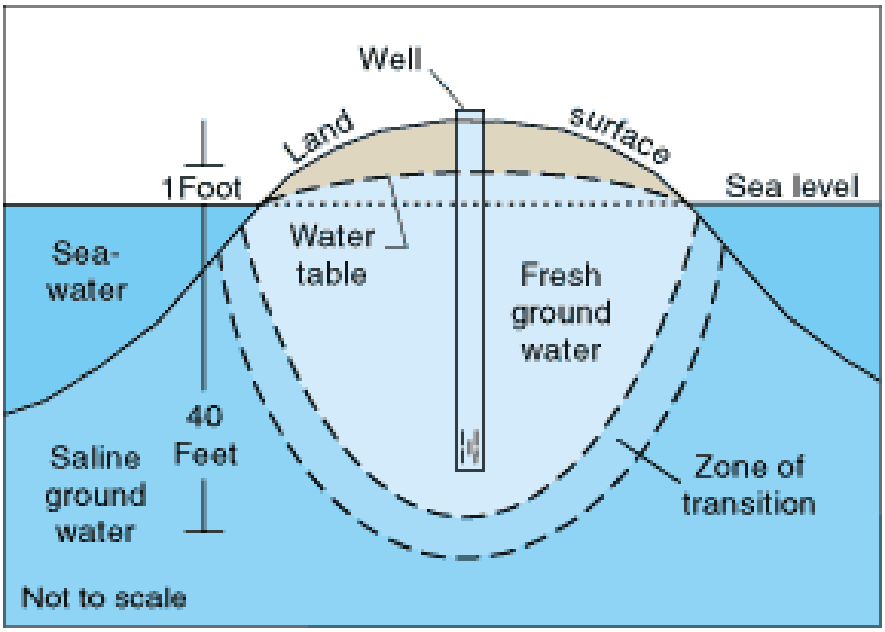

Figure 1-1. Freshwater lens on a small island. The zone of transition is the area where the sea water exchanges with the freshwater (Lyles, 2000).

Sea-level rise lead to more serious seawater intrusion in coastal and island aquifers in global range based on the expected sea level rise rate which studied in recent years (Santha Sophiya and Syed, 2013). The global mean sea-level rise rate under Representative Concentration Pathway (RCP) 8.5 is expected to be 0.82m from 2081 to 2100. Even in some specific areas such as East Sea, the expected sea-level rise can be 1.08m under RCP 8.5 scenario. (Jong et al., 2018).

Many researchers have studied the effects of sea-level rise and seawater intrusion. Masterson and Garabendian (2007) have researched the effects of sea-level rise on groundwater flow in a coastal aquifer affected by surface water. They found that the freshwater lens thickness was decreased by 2% located far from the stream, and the thickness can be decreased by 22 % to 31% near the stream with the same period and

same sea-level rise rate. The reason is the stream was tidal can be controlled by the net decline in water levels relative to local sea-level rise rate. In 2011, Abd-Elhamid and Javadi made a study which focused on the groundwater with over-pumping and saltwater intrusion in coastal areas. They considered three different scenarios which are sea-level rise, decline in groundwater table due to over-pumping, and the combination of sea-level rise and over-pumping. The results showed the last scenarios have the greatest impact which leaded to further inland movement of the transition zone. Unsal, Yagbasan & Yazicigil (2014) indicted the sloping land surface resulting in inward migration of the coastal boundary and transient response of the system by pumping on a circular island with sea-level rise. Four scenarios which have different recharge or sea-level rise combinations are determined in this research. The results indicated highest pumping rate and freshwater resource occurred in the "no change in both recharge and sea level" scenario, and lowest pumping rate and freshwater resources occurred in the "decreasing recharge accompanied by the sea-level rise" scenario.

Previously, many studies have indicated the freshwater volume can decrease on islands caused by sea level rise (Rotzoll, Oki & El-kadi, 2010; Rozell and Wong, 2010; White and Falkland, 2010; Vandenbohede et al., 2014; Antonellini et al., 2015, Ohwoghere-Asuma and Essi, 2017.) In 2016, Gulley et al. indicated the freshwater lens shape and volume could be affected by expansion of lakes on islands due to sea level rise. When the sea level rise, the lake width grows and cause more lake surfaces can be exposed to the sun. Therefore, the evaporation in the lake will increase. After that, the constant precipitation and increased evaporation in the lake resulting in reduced the recharge of

the freshwater lens, cause the freshwater lens volume reduced. Also, the expanded lake will reduce the land surface, which also limited the volume of the freshwater lens. Figure 1-2 displays steady-state simulation results of the freshwater lens volume.

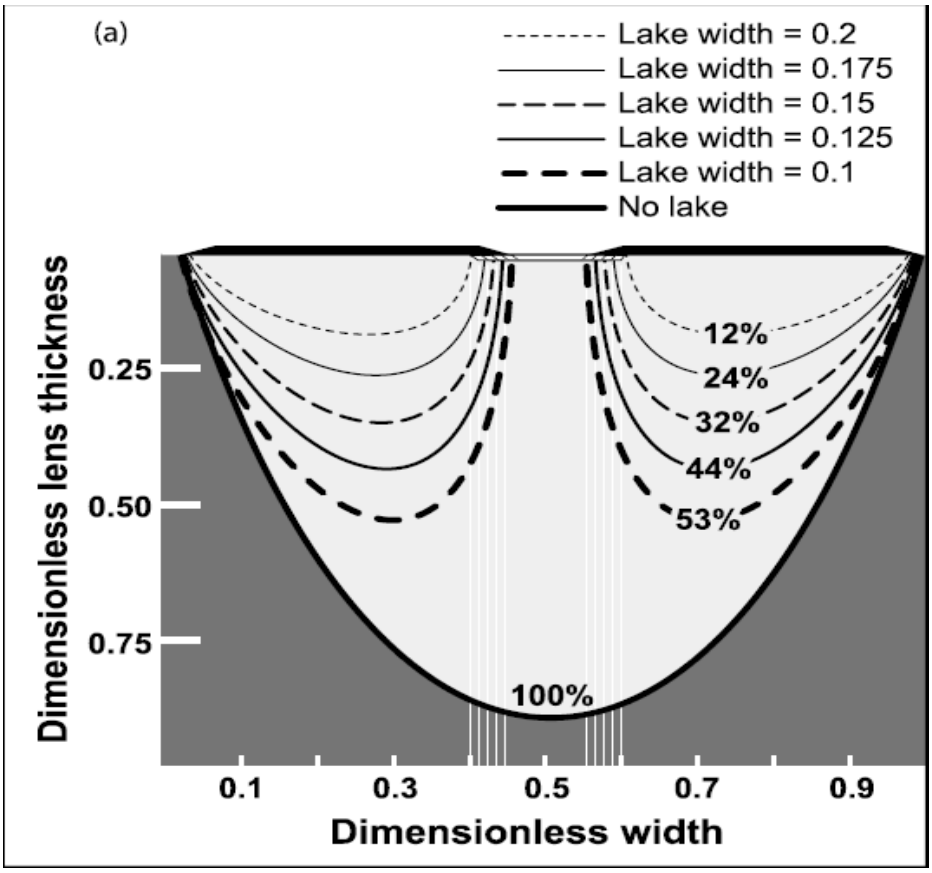

Figure 1-2. Comparison of lake formation scenarios on freshwater lens volume. This dimensionless island only exhibited drinking water in the freshwater lens. The normalized lateral distance is 1000 m width and the vertical distance is the maximum depth of the seawater (TDS = 35 kg/m^3 or dimensionless TDS = 50) or dimensionless contour for the non-lake case (11 m) (Gulley et al., 2016).

Islands in the Bahamas archipelago are the prototype of the hypothetical island in this study. The Bahamas are located in southern Florida (US), contain nearly 700 islands and the scale of the island can be extensively from 9 square miles to the 2300 square miles. (Roebuck, 2004) These islands are mainly formed of limestone (Vacher and Wallis, 1992) so that the carbonate platforms continued to grow subsurface in the southern archipelago. Due to this reason, the shape of the islands is different, such as some islands in the northern are quite narrow. (Melim and Masaferro, 1997). The Bahamas islands have a unique rainfall distribution so that the climate in this archipelago changed seasonally. (Vacher and Wallis, 1992; Whitaker and Smart, 1997) In Figure 1-3, the island in the Bahamans is naturally divided into some rainfall zones and the precipitation decrease from north to south significantly.

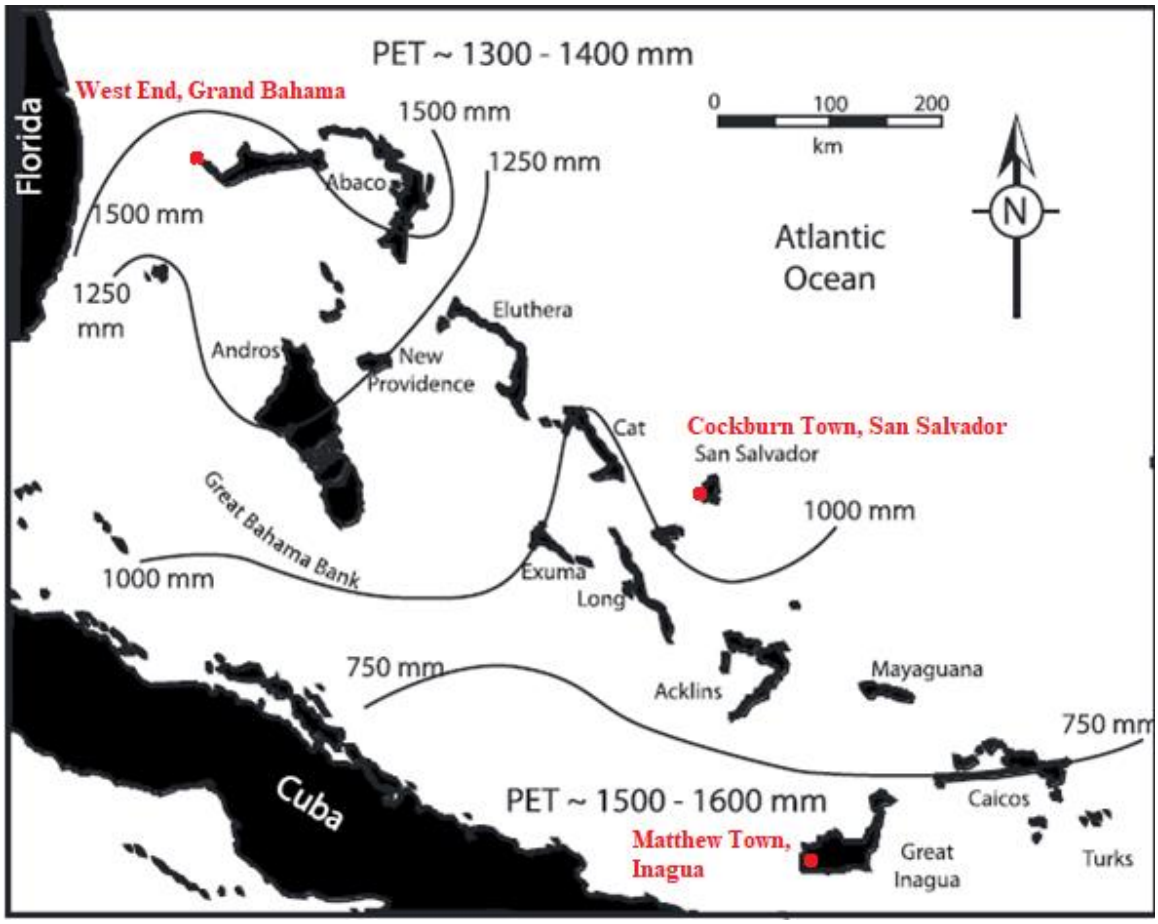

Figure 1-3. Precipitation and potential evapotranspiration distribution of the Bahamas. The precipitation varies in gradients because the precipitation decreased with latitude decrease (Gulley et al., 2016).

In order to study the freshwater lens, direct field studies and numerical modeling are widely used. Compared to the direct field study, numerical modeling can easily simulate the change process and adjust the parameters for different situations. Vandenbohede and Lebbe (2002) used numerical modeling to study the impact of hydraulic conductivity on the depth of the freshwater lens. Lin et al. (2009) used SEAWAT, a numerical modeling program, to study the seawater intrusion in the Alabama Gulf Coast. USA. Guha (2010)

studied saltwater intrusion in a coastal aquifer in response to the sea-level rise by setting up the two- and three- dimensional variable-density groundwater flow models. Bailey, Jenson & Olsen (2010) estimated the thickness of the freshwater lens of atoll island though numerical model. Sarva et al. (2011) used SEAWAT to define the seawater intrusion in Manukan Island, East Malaysia. Loáiciga et al. (2012) had modeling simulation on the sea water intrusion in coastal aquifers in order to present a method to assess the contributions of 21st century sea-level rise rate. Seyf-laye et al. (2012) setted up a three-dimensional groundwater flow model to evaluated the contaminant transportation in Beijing area. Chen et al. (2013) estimated the recharge of Pingtung Plain by numerical modeling which combined with the integrating water table fluctuation method. El Alfy (2014) used numerical modeling tools for managing the groundwater resources in arid areas. Abd-Elaty, Hany Farhat & Javadi (2016) also researched on the effects of changing hydraulic parameters on saltwater intrusion in coastal aquifers by using SEAWAT.

From above numerous literature reviews, it could be seen there are many pieces of research focuses on the relationship of groundwater, freshwater lens, seawater intrusion, sea-level rise, geological parameter and even topography, but no one focuses on the impact of freshwater lens volume on a narrow island combined with the different sea-level rise rate with lake expansion and dynamic climate condition in gradients. Therefore, the purpose of this research is using numerical modeling method to simulate the freshwater lens depletion rate and salinity in response to a range of sea-level rise rates and climate gradients with lake expansion for small islands for long-term transient simulation in SEAWAT.

1.2 Methods

The commonly used groundwater flow and transport simulation software, SEAWAT (Guo and Langevin, 2002) is used in this study. SEAWAT is a program that combines with the code from the MODFLOW and MT3DMS to solve the three-dimensional, variable-density groundwater flow problem. SEAWAT uses either an explicit or implicit procedure to couple the ground-water flow equation with the solute-transport equations. It has many kinds of packages to describe the physical parameters in groundwater modeling and simulating the transient groundwater flow by using the partial differential equation for variable-density ground-water flow in porous media. SEAWAT is widely used in coastal and island aquifer modeling in many research directions such as sea-level rise and seawater intrusion (Masterson and Garabedian, 2007; Lin et al., 2009; Rozell and Wong, 2010; Unsal, Yagbasan and Yazicigil, 2014).

The hypothetical island used here is derived from Gulley et al. (2016). This hypothetical island is imagined as a cross-section of a long barrier island, with dimensions of 1000-meters in width and 40-meters in depth, and a lake at the center of the island. Figure 1-4 shows the conceptual water balance for the lake and land surface. The lake evaporation, *E*, is calculated with the Vapor-Pressure Relations (Dingman, 2015):

$$e_s = e^*(T) = 0.611 \cdot exp\left(\frac{17.3 \cdot T}{T + 237.3}\right) \quad (1)$$

$$e(z) = RH(z) * e^*(T(z)) \quad (2)$$

$$E = 1.20 \times 10^{-6} \cdot \frac{u(z_m) \cdot [e_s^* - e_{(z_m)}]}{\left[ln\left(\frac{z_m - z_d}{z_0}\right)\right]^2} \quad (3)$$

where *RH(z)* is relative humidity, *z* is wind speed, Equation (3) is also used to calculate the calculated potential evapotranspiration, *PET*, from the land surface. However, due to the leaf conductance and soil-moisture deficit in land surface (Dingman, 2015), the actual evapotranspiration (*AET*) of the land surface cells equals the potential evapotranspiration (*PET*) times a factor, *f*, which is assumed here as *f* = 0.25.

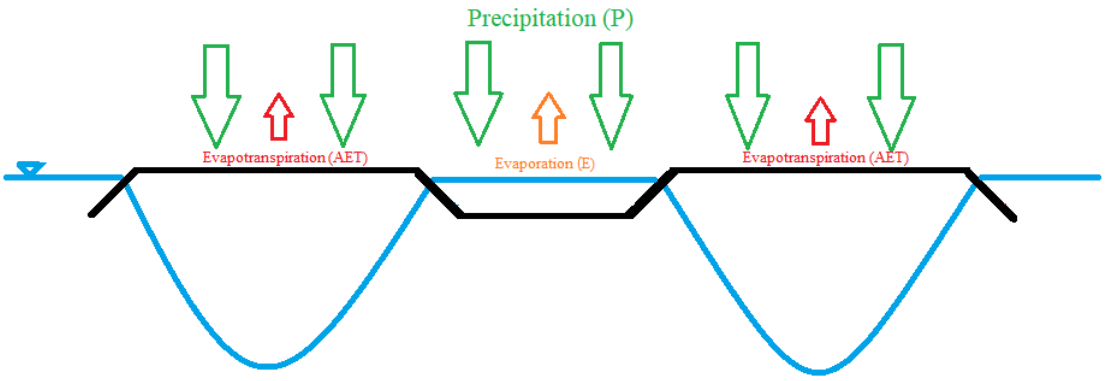

Figure 1-4. Simple water balance diagram in a small island. The evaporation (*E*) of the lake equals to the potential evapotranspiration (*PET)* and the actual evapotranspiration (*AET*) of the land surface equals to the potential evapotranspiration (*PET*) times a factor (*f*)=0.25 (*E=PET*, *ET= f·PET*) (Dingman, 2015).

To represent the climate gradient in the Bahamas, rainfall and temperature data are chosen from three sites, located in Matthew Town on Inagua island, Cockburn Town on San Salvador island and West End on Grand Bahama island, which all showed in Figure

1-3. All the rainfall and temperature data were measured from 1961 to 1990 daily. Daily wind speed, vapor pressure and humidity data from the three sites is available only for the Cockburn Town site from 1970 to 1985. The daily wind speed, vapor pressure and humidity data from Cockburn Town station are assumed to be similar for all three sites and were used to calculate the lake evaporation, *E*.

Table 1-1 displays the average annual precipitation, the computed results of lake evaporation, actual evapotranspiration in the land, and the effective recharge of the lake and the land surface for all the three sites. The data in this table are calculated based on the raw data given by the Bahamas Water Authority (2018). Also, these data are been used to calculate the average monthly precipitation, evaporation and actual evapotranspiration of these sites, and used to present the seasonal dynamic in Figure 1-5. For example, both Inagua Island and San Salvador Island have two wet seasons which are from April to June and September to October, and dry season belongs to the other month. However, Grand Bahama only has one wet season which is from June to October.

Table 1-1. Average annual climate data from the three sites in the Bahamas. The sources of the data are come from Bahamas Water Authority (2018).

Island	Precipitation Rate (P, mm/yr)	Lake Evaporation Rate (E, mm/yr)	Effective Lake Recharge Rate (mm/yr)	Actual Evapo-transpiration Rate (AET, mm/yr)	Effective Land Surface Recharge Rate (mm/yr)
Inagua	659	1260	-601	315	344
San Salvador	998	1234	-236	309	689
Grand Bahama	1282	1095	187	274	1008

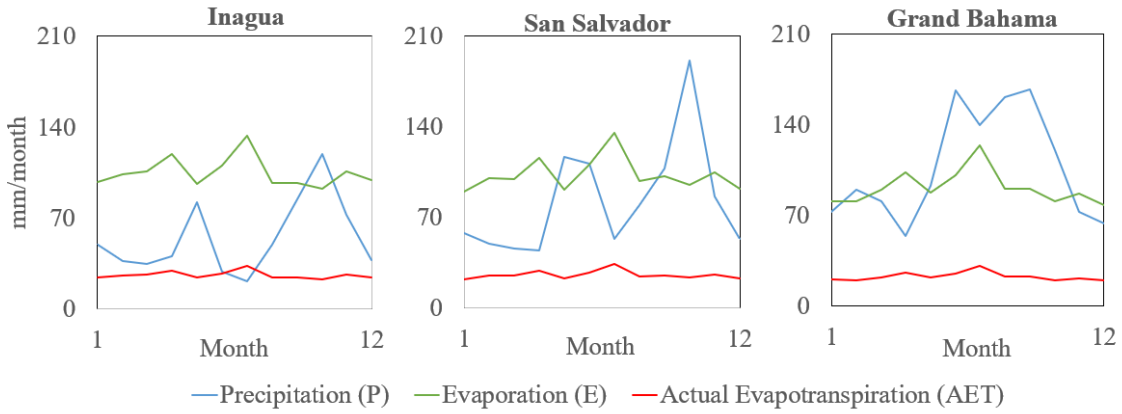

Figure 1-5. Seasonal dynamic of three islands: the wet and dry seasons were compared by the precipitation, potential evapotranspiration, and effective recharge of the lake for these islands.

Table 1-2 shows the physical and chemical parameters used in the model, all of which are derived from Gulley et al. (2016). The number of grid cells in x-, y- and z-direction is 1000, 1 and 40, respectively, giving grid cell sizes of 1 m^3. The depth of the domain is set so that the bottom boundary condition of no-flow and no-concentration flux does not affect the freshwater lens dynamics. The left and right boundaries are set to constant head (sea level, head = 0) and constant concentration (seawater concentration = 35 kg/m3). The top boundary is set at no-flow and no-concentration flux. On the other hand, the lake cells are set as the effective porosity equal to 1 and horizontal hydraulic conductivity equal to 100 m/day, instead of effective porosity equal to 0.3 and horizontal hydraulic conductivity equal to 50 m/day in the non-lake cells. The freshwater lens volume is defined as the volume of groundwater with a concentration less than 1 kg/m^3, which are defined by the USGS (Howard Perlman, 2018).

Table 1-2. Input parameters in SEAWAT simulation.

Physical parameters		
Width	1000	m
Thickness	1	m
Height	40	m
Seawater concentration	35	kg/m^3
Freshwater concentration	<1	kg/m^3
Horizontal hydraulic conductivity (land cells)	50	m/day
Horizontal hydraulic conductivity (lake cells)	100	m/day
Vertical hydraulic conductivity	10	m/day
Longitudinal dispersivity	0.1	m
Traversie dispersivity	0.01	m
Vertical dispersivity	0.05	m
Molecular diffusivity	0	$kg/m^2/day$
Specific Storage	0.003	1/m
Specific Yield	0.3	
Effective porosity (land cells)	0.3	
Effective porosity (lake cells)	1	
Numerical parameters		
Δx	1	m
Δy	1	m
Δz	1	m
Number of time step (Primitive lake formation)	5000	
Total time (Primitive lake formation)	100,000	Day
Number of time step (Sea-level rise and climate condition simulation)	100	
Total time (Sea-level rise and climate condition simulation)	30	Day
Initial condition of primitive lake formation		
Initial concentration	1	kg/m3
Initial head	0	m
Initial lake width	100	m

According to Forbes et al. (2013) projected sea-level rise rates for 18 selected islands from 2010 to 2100, including the Bahamas chain, indicating that the Bahamas are expected to experience relatively low sea level rise rates compared to other island chains. Three sea level rise rates were selected from Forbes et al. (2013) to give a low projected

rate (0.56 mm/yr), a medium projected rate (6.22 mm/yr) and a high projected rate (11.78 mm/yr). The lowest sea-level rise rate is the underestimate future sea levels in a non-fossil fuel case which established by IPCC in 2007. The medium sea-level rise rate corresponds to an upper limit projection for the fossil fuel intensive with the contribution of accelerated glacier outflow from the major ice sheets. The highest sea-level rise rate is the maximum prediction value of the local area that based on the 1.15m global mean sea-level in the past 90 years.

The slopes of the shoreline and the interior depression holding the lake were set to 0.004 m/m, which Gulley et al. (2016) also used in his study (see Figure 1-6). In the simulations, as sea level rises, the shoreline is inundated and the lake expanded. According to the topography, sea level rise rate, and cell size in the lateral direction, shoreline cells are lost and lake cells are gained at a constant rate, although the discrete nature of the finite-difference cells gives rise to an integer change rather than a continuous change, as shown in Figure 1-6.

Figure 1-6. Simple lake expansion and shoreline inundation diagram in a small island. When sea level rise to the light blue position, the lake cells expanding on both side and the land cell tighten from both sides. Due to this reason, the starting position of the lake move to the left and the lake cells increased. On the other hand, the land cells on both side transfer to the constant concentration and head boundary.

Numerical simulations were conducted for the three climates representative of Inagua, San Salvador, and Grand Bahamas islands and three sea level rise rates, for total of 9 simulations. In order to compare the effects of lake expansion on the quality of the freshwater lens, another 9 simulations, which the lake width are fixed, called the non-lake expansion cases have been established. Each numerical simulation was separated into a "spin-up" part and a sea level rise part. In the first part, the model was simulated with a given monthly time series for *P*, *E*, and *AET* in the transient mode for 273 years until the results reached the steady state. This process was used to simulate the initial formation of the lake in the center of the hypothetical island. In the second part, a 50-year numerical simulation was conducted with the steady-state simulation from the spin-up period as an initial condition, the same climate time series used in the spin-up period, and a rising sea level. Time steps of 1 month for both parts were selected based on the Courant number (*Cr*) constraint less than or equal to 1 because this number is a dimensionless number to accelerate convergence and enhance the model stability. In this case, $Cr = (v * \Delta t)/\Delta x$, where *v* is the velocity, Δt is the time step, and Δx is the width of a cell (Giraldo, 2018). These simulations were run in a time series which combined with the time-varying boundary condition and 1-year cyclic evapotranspiration and recharge condition. These simulations were run in the transient mode for every 30 days by reading the head and concentration condition from the original homogenous lake. Then, the evapotranspiration and recharge data of both lake and land surface, the number of new lake cells, the starting and ending position of new lake cells, and the number of constant head and concentration boundary cells would be modified in input files to accord with the real situation. The results of groundwater head and concertation from the previous month simulation would

be used in next period simulation, and all the other physical alterable parameters would be changed again. The detailed input files preparation and modeling execution process in SEAWAT were displayed in Appendix A.

1.3 Results and Discussion

According to the methods section, 18 cases were simulated which included three different climate conditions, three different sea-level rise conditions and lake-expansion vs. non-lake expansion cases. The simulation results are plotted in Figure 1-7. Note that the Inagua island climate condition combined with 11.78mm sea-level rise rate in lake expansion scenario stopped at the 425th month, due to numerical errors that exceeded error criteria. In the 424th month, the freshwater lens depletion is 97%, which can be considered as the freshwater lens has almost exhausted.

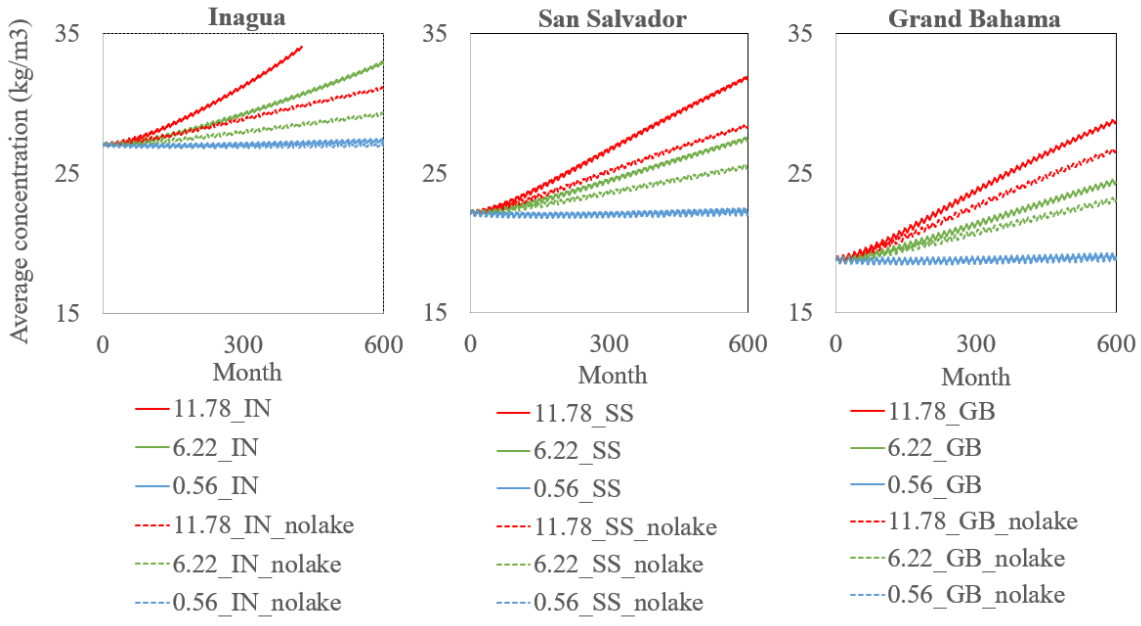

Figure 1-7. Average concentration vs. time. The legend of this figure is used to distinguish islands and sea-level rise rates: the red lines are Inagua Island (the northern island), the green lines are San Salvador Island (central island), the blue lines are Grand Bahama Island (southern island). All the solid lines represent the lake expansion scenarios and all the dash lines represent the non-lake expansion scenarios. The y-axis is represented as the average salinity concentration for whole island in kg/m^3.

The Figure 1-7 indicates the average concentration, which is also called salinity, in the entire island for all the cases in the 600-month (50-years) simulation. Generally, the average concentration of all cases indicates the steady upward trends in the 50-year simulation, but the salinity also has a slightly decreasing trend in some months in the 1-year cyclical period. This fluctuating period always occurred with the seasonal climate condition in their related island, and the magnitude of this oscillation changes as the recharge changes in each month.

On the other hand, the average concentration of all cases has a different rising rate, which means they have different slopes. According to this figure, the cases with 11.78mm sea-level rise rate usually have the fastest upward trend, and the cases with 0.56mm sea-level rise rate have the slowest rising trend which almost close to 0. The cases with lake expansion scenarios have faster upward trend than the non-lake expansion scenarios under the 11.78mm and 6.22mm sea-level rise rate condition. However, the upward trends are not obvious for both lake and non-lake condition under the 0.56mm sea-level rise rate condition. The reason is the progress of coastal intrusion under low sea-level rise rate is too slow so that the simulation results will not change too much. Meanwhile, the

starting position of the average concentration in Inagua Island is also higher than the other two islands because Inagua Island has the driest climate condition so that the initial freshwater lens volume is smaller than the other two islands.

Table 1-3. Slope of salinity from 300th-month to 425th-month for all cases.

	Slope of Salinity (kg/m3/month)
11.78_IN	0.0222
11.78_IN_nolake	0.0077
6.22_IN	0.0113
6.22_IN_nolake	0.0043
0.56_IN	0.0009
0.56_IN_nolake	0.0002
11.78_SS	0.0180
11.78_SS_nolake	0.0115
6.22_SS	0.0102
6.22_SS_nolake	0.0064
0.56_SS	0.0008
0.56_SS_nolake	0.0004
11.78_GB	0.0181
11.78_GB_nolake	0.0142
6.22_GB	0.0105
6.22_GB_nolake	0.0008
0.56_GB	0.0008
0.56_GB_nolake	0.0006

Two special cases, which are the 11.78mm and 6.22mm sea-level rise rate and Inagua Island climate condition and combined with the lake expansion scenario, displayed a non-linear trend. In order to avoid the impact of these two special cases on the results, the slope calculation range has been selected from 300th-month to 425th-month because the slopes of the two cases in this interval can be approximated as linear. Therefore, Table 1-

3 is to summarize the slope of salinity for all cases. All slopes are estimated by the linear regression equation and the value is consistent with the trend in Figure 1-7.

Figure 1-8 demonstrates the recharge process of lake, land and entire island from two cases. The left case has the highest sea-level rise rate and driest climate condition, and the right case has the lowest sea-level rise rate and wettest climate condition. Based on the high sea-level rise rate, the left case has much quicker lake expansion progress than the right case, resulting in a larger amplitude than the right case. However, the left case has the direst climate condition, so the lake will evaporate more water in the dry season and have less precipitation in the wet season, which leads to a larger negative recharge in the lake. So the recharge of the lake on the left side has the decreasing slope. On the opposite, the case at right side can get enough recharge of the lake for a long time, so the amplitude does not change with the time significantly. Comparing the recharge of land and entire island, the recharge of the left case also reduced faster than the right side due to the faster land loss and drier climate condition. Therefore, all the slopes for the left case are negative which mean the recharge of the entire island decreases with time. Although the slopes of recharge of land and entire island for the right case are negative, these negative numbers are quite small so that they can be ignored. Therefore, the recharge of the entire island for right case does not seem to change with the time.

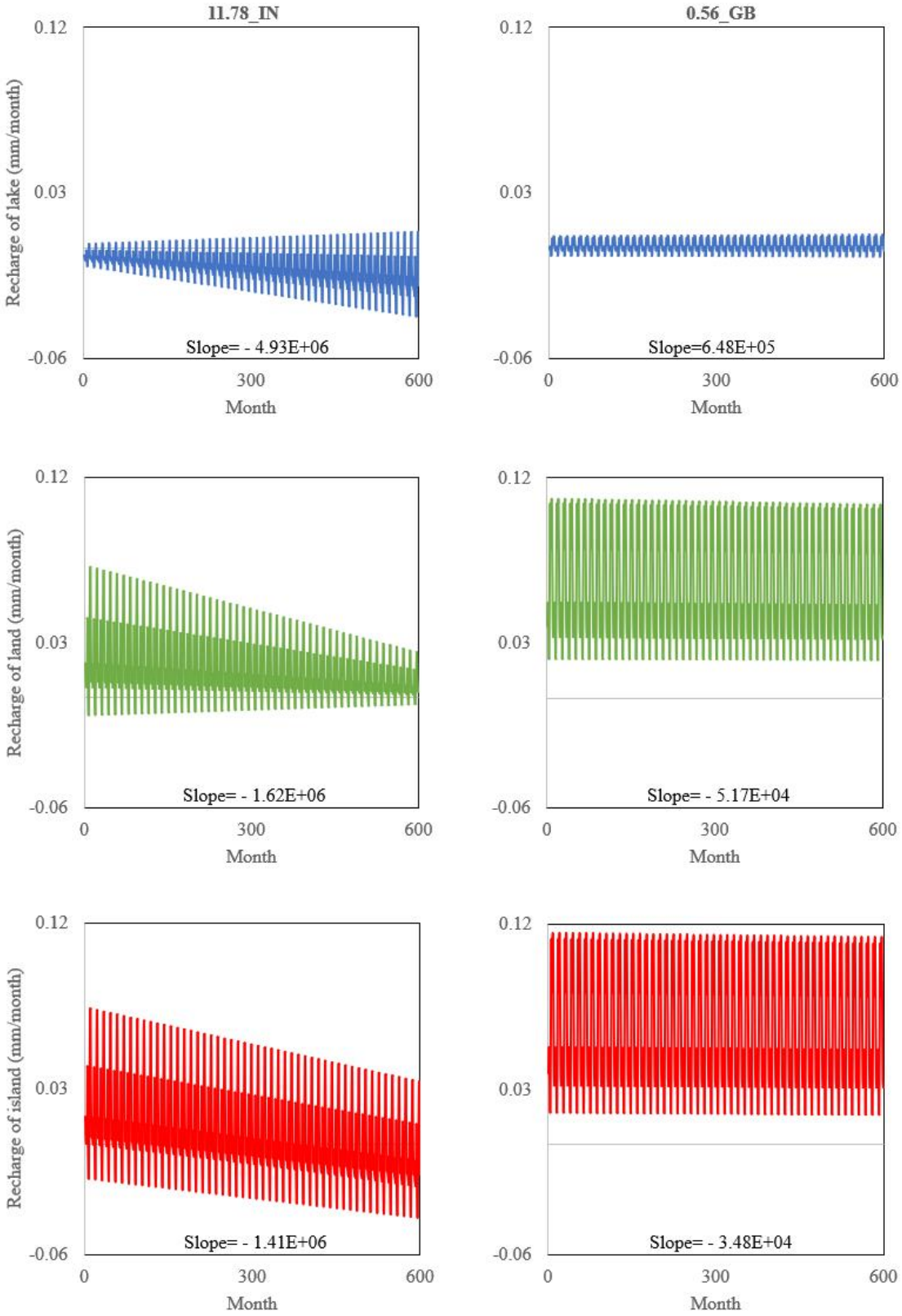
11.78_IN
0.56_GB
Recharge of lake (mm/month)
Recharge of land (mm/month)
Recharge of island (mm/month)
0.12
0.03
-0.06
0
300
600
Month
Slope= - 4.93E+06
Slope=6.48E+05
Slope= - 1.62E+06
Slope= - 5.17E+04
Slope= - 1.41E+06
Slope= - 3.48E+04

Figure 1-8. Recharge of lake, land and entire island and related slope for two selected cases. The y-axis is represented as the computed recharge of lake, land and entire island in the unit of mm/month, so the slope shown in the figures have been calculated based on the original slope from the linear regression equation times 600 months. The reason for this is to eliminate the unit of slope become in/month/month.

Figure 1-9 illustrated the only Grand Bahama Island always has a positive recharge in the lake, land and entire island for the three sea-level rise situations because of the wettest climate condition. Also, Inagua Island has the largest negative recharge value in the lake because of the driest climate condition. Although both Inagua Island and San Salvador Island have the negative recharge in the lake, the recharge in the land is still positive and offset the impact of the negative recharge in the lake, leads to a positive recharge in the entire island. Comparing the recharge at the different sea-level rise rate in three islands, the 0.56mm sea-level rise rate always has the highest positive recharge in land and the entire island due to the slow intrusion in the coastal and slow expansion progress of lake. Comparing the recharge between the lake expansion and non-lake expansion scenario, since the recharge in lake will not change in non-lake expansion, the recharge in entire island of non-lake expansion scenarios are higher than the recharge of lake expansion scenarios.

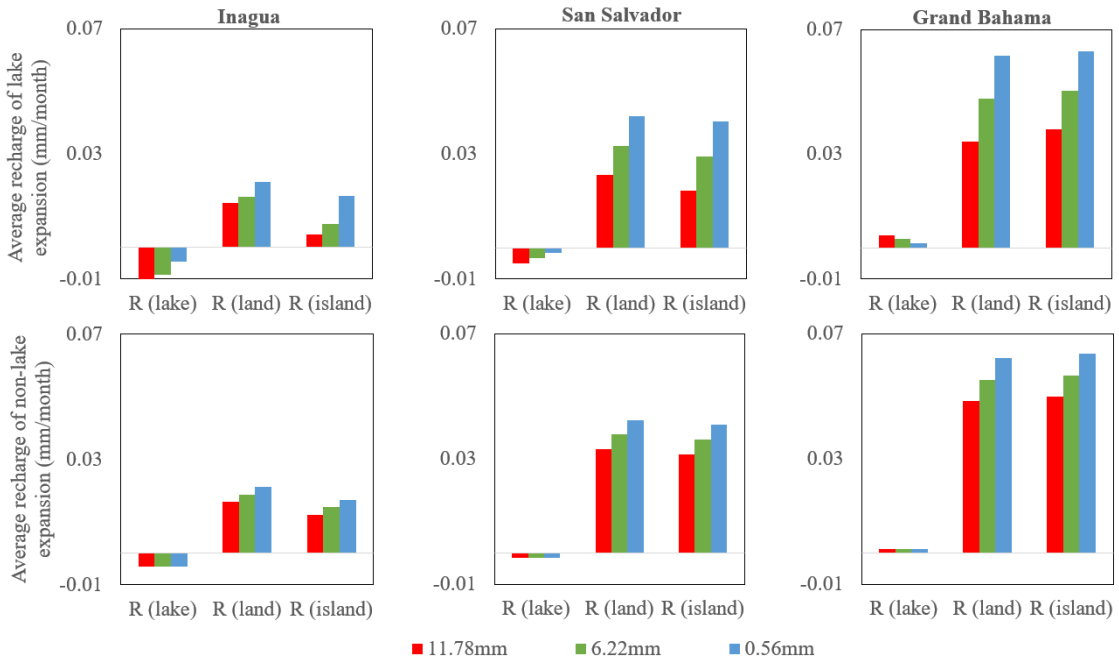

Figure 1-9. The monthly average recharge of the lake, land, and the entire island for three selected islands. The legend of this figure is used to distinguish the sea-level rise rates: the red block is 11.78mm, the green block is 6.22mm and the blue block is 0.56mm. The y-axis is represented as the monthly average recharge for both lake and non-lake expansion scenarios in the unit of mm/month.

Table 1-4. The ratio of the width of lake and land at the end of 50-year simulation to the width of lake and land at the initial condition.

Sea-level rise rate (mm/yr)	**L(lake) at the end (m)/ L(lake) in the beginning (m)**	**L(land) at the end (m)/ L(land) in the beginning (m)**
11.78mm (lake expansion)	3.94	0.35
11.78mm (non-lake expansion)	1.00	0.67
6.22mm (lake expansion)	2.55	0.66
6.22mm (non-lake expansion)	1.00	0.83
0.56mm (lake expansion)	1.13	0.97

0.56mm (non-lake expansion)	1.00	0.98

Table 1-4 shows the ratio of the lake and land width at the end of 600 months to the lake and land width at the initial condition for all the sea-level rise conditions in both lake expansion and non-lake expansion scenarios. For the lake expansion scenarios, the higher sea-level rise rate would cause the faster lake expansion and more convenient coastline erosion. Relatively, higher sea-level rise rate also leads to quicker land loss. Compare to the non-lake expansion scenarios, the lake width does not change at all, but the land width is still decreasing due to the coastal intrusion. However, the rate of reduction of non-lake expansion scenarios is still less than the lake expansion scenarios.

1.4 Conclusion

This study focused on the freshwater lens volume and average concentration which response to the range of sea-level rise rates, climate gradients and lake or non-lake expansion scenarios for different 18 cases. The 50-year transient simulations were set up in SEAWAT. The climate data were computed from the 15-year monthly precipitation data for three different islands in the Bahamas, which the location displayed the gradual drought condition from north to south due to the geological conditions. The wide range sea-level rise rate which from 0.56 mm/yr to the 11.78 mm/yr, was chosen from the different simulated scenarios.

According to the simulation results, one case stopped at 425th month due to the exhausted freshwater lens. Except for this special case, the other 17 cases were simulated

for 50 years. According to the figures and tables shown in above section, the following point can be concluded:

1. All cases presented the upward trend of the average concentration, which also called salinity. the upward trend has the oscillation in a cyclical period, the magnitude of the oscillation change accord with the season climate condition in their related island, which means the freshwater lens can be a response in the seasonal climate conditions.
2. The slope of salinity for all the case is positive but have a different value. The cases with 11.78mm sea-level rise rate usually have the fastest upward trend which means the highest slope, and the cases with 0.56mm sea-level rise rate have the slowest rising trend which the slope almost equal to 0. The lake expansion scenarios also have a faster upward and larger slope than the non-lake expansion scenarios. However, for the lowest sea-level rise rate of 0.56mm, the difference for both lake and non-lake expansion scenarios in three islands are not obvious due to the slow progress of coastal intrusion.
3. The initial position of the average concentration in Inagua Island is higher than the other two islands. The reason is that the Inagua Island has the driest climate condition so that the initial freshwater lens volume is smaller than the other two islands. On the opposite, the Grand Bahama Island has the lowest starting position in salinity plot.
4. Only Grand Bahama Island has a positive recharge in the lake, land and entire island for all three sea-level rise situations because the island has the wettest

climate condition. Inagua Island has the largest negative recharge value in the lake because of the driest climate condition. All the islands have the positive recharge in the entire island because the recharge of land can offset the negative recharge of the lake.

5. The 0.56mm sea-level rise rate always has the highest positive recharge in land and the entire island because the coastal intrusion and lake expansion progress is slow. With the constant recharge of the lake in the non-lake expansion case, the recharge of the entire island of non-lake expansion scenarios is higher than the recharge of lake expansion scenarios.
6. Higher sea-level rise rate would cause the faster lake expansion and more convenient coastline erosion and land loss in both lake and non-lake expansion scenarios. Since the lake width does not change in non-lake expansion scenarios, the land loss rate of non-lake expansion scenarios is slower than the lake expansion scenarios under the same sea-level rise rate.
7. Although the results show that the sea-level rise rate, the climate condition, and lake expansion or non-lake expansion scenarios can affect the volume of freshwater lens and salinity of the entire island, this result is still a theoretical derivation so that it cannot use into the actual case directly. The reason is that many parameters are an idealized assumption so that they do not reflect the actual conditions such as the geographical condition of the island. Therefore, a significant objective needs to be studied in the future is the factor(f), which means the ratio of evapotranspiration value to the potential evapotranspiration. Since the factor used in these simulations is 0.25, it may not accord with the real geography.

0.25 is a universal value for tropical whether based on the floristics type and the area covered by the plants on land. However, the plants' species and coverage of each island in the Bahamas are not exactly same. Moreover, the climate condition also affects the factor so that the value may be overestimated or underestimated. For instance, the wettest island that located at the north of these three islands may have more land area coved by plants than the other two, so the evapotranspiration in this island could be higher than the other two islands. Therefore, the factor of the ratio of evapotranspiration to the potential evapotranspiration should larger than 0.25.

8. Another goal which needs to be focused on the future is finding an appropriate method to scale the results. The reason is to determine the proportion of coastal erosion and lake expansion caused by the sea-level rise in the volume of freshwater lenses and scale to a directly results in the vertical direction. The advantage of this visually scaling process is help decision maker understand the results easily in decision making, such as used to determine the location and height of the drinking wells within the 50-year lifetime.

2 Reference List

Abd-Elaty, I., Hany Farhat, A. E., & Javadi, A. (2016). Numerical analysis of the effects of changing hydraulic parameters on saltwater intrusion in coastal aquifers. *Engineering Computations, 33*(8), 2546-2564. doi:http://services.lib.mtu.edu:2080/10.1108/EC-11-2015-0342

Abd-Elhamid, H., & Javadi, A. A. (2011). Impact of sea level rise and over-pumping on seawater intrusion in coastal aquifers. *Journal of Water and Climate Change, 2*(1), 19-28. doi:http://dx.doi.org/10.2166/wcc.2011.053

Abd-Elhamid, H. (2017). Investigation and control of seawater intrusion in the eastern nile delta aquifer considering climate change. *Water Science & Technology, 17*(2), 311-323. doi:http://dx.doi.org/10.2166/ws.2016.129

Antonellini, M., Allen, D. M., Mollema, P. N., Capo, D., & Greggio, N. (2015). Groundwater freshening following coastal progradation and land reclamation of the po plain, italy. *Hydrogeology Journal, 23*(5), 1009-1026. doi:http://dx.doi.org/10.1007/s10040-015-1263-0

(Bahamas Water Authority, personal communication, May 13, 2018)

Bailey, R. T., Jenson, J. W., & Olsen, A. E. (2010). Estimating the ground water resources of atoll islands. *Water, 2*(1), 1-27. doi:http://services.lib.mtu.edu:2080/10.3390/w2010001

Barlow, P. M., & Reichard, E. G. (2010). Saltwater intrusion in coastal regions of north america. *Hydrogeology Journal, 18*(1), 247-260. doi:http://dx.doi.org/10.1007/s10040-009-0514-3

Chen, Y., Tsai, J., Chang, L., Wang, Y., Chen, Y., Chiang, C., . . . Chen, J. (2013). Integrating water table fluctuation method and groundwater numerical modeling on the estimation of regional recharge quantity of pingtung plain. *Geophysical Research Abstracts, 15*, Abstract EGU2013-3720. Retrieved from https://services.lib.mtu.edu:5003/docview/2116104653?accountid=28041

Dingman, S. L. (2015). *Physical hydrology* (3rd ed.). Long Grove, IL: Waveland Press, 282pp.

El Alfy, M. (2014). Numerical groundwater modelling as an effective tool for management of water resources in arid areas. *Hydrological Sciences Journal, 59*(6), 1259-1274. doi:http://services.lib.mtu.edu:2080/10.1080/02626667.2013.836278

Fratesi, B. (2013). Hydrology and Geochemistry of the Freshwater Lens in Coastal Karst. *Coastal Karst Landforms.* Coastal Research Library, 59-75. doi:10.1007/978-94-007-5016-6_3

Giraldo, F. (2018). [online] Faculty.nps.edu. Available at: http://faculty.nps.edu/fxgirald/projects/nseam/nps/new_section4.pdf [Accessed 7 Dec. 2018].

Green, N. R., Macquarrie, K. T., & B. (2014). An evaluation of the relative importance of the effects of climate change and groundwater extraction on seawater intrusion in coastal aquifers in atlantic canada. *Hydrogeology Journal, 22*(3), 609-623. doi:http://dx.doi.org/10.1007/s10040-013-1092-y

Guha, S. (2010). *Variable-density flow models of saltwater intrusion in coastal landforms in response to climate change induced sea level rise and a chapter on time-frequency analysis of ground penetrating radar signals* Retrieved from https://services.lib.mtu.edu:5003/docview/876227418?accountid=28041

Gulley, J. D., Mayer, A. S., Martin, J. B., & Bedekar, V. (2016). Sea level rise and inundation of island interiors: Assessing impacts of lake formation and evaporation on water resources in arid climates. *Geophysical Research Letters, 43*(18), 9712-9719. doi:10.1002/2016gl070667

Guo, W., & Langevin, C.D. (2002). *User's guide to SEAWAT: A computer program for simulation of three-dimensional variable-density ground-water flow*. Open-File Report 01-434, U.S. Geological Survey, Tallahassee, Florida

Howard Perlman, U. (2018). *Saline water, USGS Water-Science School*. [online] Water.usgs.gov. Available at: https://water.usgs.gov/edu/saline.html [Accessed 7 Dec. 2018].

Huang, P., & Yung-Chia Chiu. (2018). A simulation-optimization model for seawater intrusion management at pingtung coastal area, taiwan. *Water, 10*(3), 251. doi:http://dx.doi.org/10.3390/w10030251

Jong, A. C., Lim, C., Kim, D., & Jin, S. K. (2018). Assessing impacts of climate change and sea-level rise on seawater intrusion in a coastal aquifer. *Water, 10*(4), 357. doi:http://dx.doi.org/10.3390/w10040357

Kalaoun, O., Jazar, M., & Bitar, A. A. (2018). Assessing the contribution of demographic growth, climate change, and the refugee crisis on seawater intrusion in the tripoli aquifer. *Water, 10*(8), 973. doi:http://dx.doi.org/10.3390/w10080973

Lin, J., Snodsmith, J. B., Zheng, C., & Wu, J. (2009). A modeling study of seawater intrusion in alabama gulf coast, USA. *Environmental Geology, 57*(1), 119-130. doi:http://services.lib.mtu.edu:2080/10.1007/s00254-008-1288-y

Loáiciga, H.,A., Pingel, T. J., & Garcia, E. S. (2012). Sea water intrusion by sea-level rise: Scenarios for the 21st century. Ground Water, 50(1), 37-47. doi:http://services.lib.mtu.edu:2080/10.1111/j.1745-6584.2011.00800.x

Lyles, J. (2000). Is Seawater Intrusion Affecting Ground Water on Lopez Island, Washington? Fact Sheet FS-057-00, *U.S. Geological Survey*, Tacoma, Washington.

Masterson, J. P., & Garabedian, S. P. (2007). Effects of Sea-Level Rise on Ground Water Flow in a Coastal Aquifer System. *Ground Water, 45*(2), 209-217. doi:10.1111/j.1745-6584.2006.00279.x

Melim, L. A., & Masaferro, J. L. (1997). Geology of the Bahamas: Subsurface Geology of the Bahamas Banks. *Developments in Sedimentology Geology and Hydrogeology of Carbonate Islands*, 161-182. doi:10.1016/s0070-4571(04)80025-6

Ohwoghere-Asuma, O., & Essi, O. E. (2017). Investigation of seawater intrusion into coastal groundwater aquifers of escravos, western niger delta, nigeria. *Journal of Applied Science & Environmental Management, 21*(2), 362-369. doi:http://services.lib.mtu.edu:2080/10.4314/iasem.v21i2.18

Roebuck, L. (2004). Water Resources Assessment of The Bahamas. *US Army Corps of Engineers, Mobile District & Topographic Engineering Center*, Mobile, Alabama

Rotzoll, K., Oki, D. S., & El-kadi, A. (2010). Changes of freshwater-lens thickness in basaltic island aquifers overlain by thick coastal sediments. *Hydrogeology Journal, 18*(6), 1425-1436. doi:http://services.lib.mtu.edu:2080/10.1007/s10040-010-0602-4

Rozell, D. J., & Wong, T. (2010). Effects of climate change on groundwater resources at Shelter Island, New York State, USA. *Hydrogeology Journal, 18*(7), 1657-1665. doi:10.1007/s10040-010-0615-z

Santha Sophiya, M., & Syed, T. H. (2013). Assessment of vulnerability to seawater intrusion and potential remediation measures for coastal aquifers: A case study from eastern india. Environmental Earth Sciences, 70(3), 1197-1209. doi:http://dx.doi.org/10.1007/s12665-012-2206-x

Sarva, M. P., Mohd, H. A., Ahmad, Z. A., Mokhtar, M., & Bidin, K. (2011). Numerical simulation of seawater intrusion in manukan island, east malaysia. *Journal of Modelling in Management, 6*(3), 317-333. doi:http://services.lib.mtu.edu:2080/10.1108/17465661111183711

Seyf-laye, A., Mingzhu, L., Djanéyé-bouindjou, G., Fei, L., Lyutsiya, K., Moctar, B. L., & Honghan, C. (2012). Groundwater flow and contaminant transport modeling applications in urban area: Scopes and limitations. *Environmental Science and Pollution Research International, 19*(6), 1981-93. doi:http://services.lib.mtu.edu:2080/10.1007/s11356-012-0744-0

Unsal, B., Yagbasan, O., & Yazicigil, H. (2014). Assessing the impacts of climate change on sustainable management of coastal aquifers. *Environmental Earth Sciences, 72*(6), 2183-2193. doi:10.1007/s12665-014-3130-z

Vacher, H. L., & Mylroie, J. E. (1991). Geomorphic evolution of topography lows in bermudian and bahamian islands; effects of climate. *Proceedings of the Symposium on the Geology of the Bahamas, 5*, 221-234. Retrieved from https://search.proquest.com/docview/1312832828?accountid=28041

Vacher, H. L., & Wallis, T. N. (1992). Comparative Hydrogeology of Fresh-Water Lenses of Bermuda and Great Exuma Island, Bahamas. *Ground Water, 30*(1), 15-20. doi:10.1111/j.1745-6584.1992.tb00806.x

Vandenbohede, A. A., & Lebbe, L. L. (2002). Numerical modelling and hydrochemical characterisation of a fresh-water lens in the belgian coastal plain. *Hydrogeology Journal, 10*(5), 576-586. doi:http://services.lib.mtu.edu:2080/10.1007/s10040-002-0209-5

Vandenbohede, A., Mollema, P. N., Greggio, N., & Antonellini, M. (2014). Seasonal dynamic of a shallow freshwater lens due to irrigation in the coastal plain of Ravenna, Italy. *Hydrogeology Journal, 22*(4), 893-909. doi:10.1007/s10040-014-1099-z

Whitaker, F. F., & Smart, P. L. (1997). Climatic Control of Hydraulic Conductivity of Bahamian Limestones. *Ground Water, 35*(5), 859-868. doi:10.1111/j.1745-6584.1997.tb00154.x

White, I., & Falkland, T. (2010). Management of freshwater lenses on small pacific islands. *Hydrogeology Journal, 18*(1), 227-246. doi:http://dx.doi.org/10.1007/s10040-009-0525-0

Xu, Z., Bassett, S. W., Hu, B., & Dyer, S. B. (2016). Long distance seawater intrusion through a karst conduit network in the woodville karst plain, florida. *Scientific Reports (Nature Publisher Group), 6*, 32235. doi:http://dx.doi.org/10.1038/srep32235

A Appendix

A.1 Input files preparation and modeling execution process in SEAWAT